Int. J. of Thermodynamics ISSN 1301-9724
Vol. 10 (No. 3), pp. 87-96, September 2007

A Detailed One Dimensional Finite-Volume Simulation Model of a Tubular SOFC and a Pre-Reformer*

Francesco Calise**, Massimo Dentice d'Accadia and Adolfo Palombo
DETEC-Università degli Studi di Napoli Federico II
P.le Tecchio 80- 80125 Naples. Italy.

Laura Vanoli
Dipartimento di Scienza degli Alimenti -Università degli Studi di Napoli Federico II
Via Università 100 - 80055 Portici (NA). Italy.

Abstract

In this paper, a detailed model of a Solid Oxide Fuel Cell (SOFC) tube, equipped with a tube-and-shell pre-reformer unit, is presented. Both SOFC tube and pre-reformer are discretized along their axes. Detailed models of the kinetics of the shift and reforming reactions are introduced. Energy, mole and mass balances are performed for each slice of the components under investigation, allowing the calculation of temperature profiles. Friction factors and heat exchange coefficients are calculated by means of experimental correlations. Detailed models are also introduced in order to evaluate SOFC overvoltages. On the basis of this model, temperatures, pressures, chemical compositions and electrical parameters are evaluated for each slice of the two components under investigation. Finally, the influence of the most important design parameters on the performance of the system is investigated.

Keywords: Modelling, fuel cell, solid oxide fuel cell, SOFC, tubular SOFC, SOFC pre-reformer.

1. Introduction

Solid Oxide Fuel Cells (SOFC) can be considered one of the most efficient energy conversion devices for power production in stationary applications. In fact, the main peculiarities of such systems are: high electrical and thermal efficiencies, low pollutant emissions and reliability (Singhal et al., 2003).

Presently, a number of types of SOFC are under investigation, namely: tubular, planar, tubular High Power Density (HPD) and micro-tubular (Singhal et al., 2003). Among them, the tubular configuration, developed by Siemens-Westinghouse since the 1970s, can be considered as the most mature and reliable one (Larmine et al., 2004). Nevertheless, research must solve a number of issues before its commercialization, such as: cost targets, operating life, system optimization and integration with traditional devices (DOE, 2002).

In the last few years many researchers have been involved in the investigation of such systems by means of multi-scale approaches. In fact, many papers are available in literature, dealing with the CFD or 0-D, transient or not, simulations of the SOFC stack and of power plants based on such technology (Singhal et al., 2003). Usually, CFD simulations are very time consuming both for model implementation and for calculation. On the other hand, 0-D simulations are much simpler and faster even if they cannot allow to determine parameter profiles (temperature, pressure, chemical composition, current density, etc.) within the component (Calise et al., 2004, Calise et al., 2006 a-c, Costamagna et al., 2001, Chan et al., 2002, Chan et al., 2003).

A number of 0-D models were previously implemented by the authors performing exergy analyses and optimization of hybrid SOFC power plants (Calise et al., 2004, Calise et al., 2006 a-c). In these models, some simplifying assumptions were introduced in order to accomplish the evaluation of the electrochemical performance by using a 0-D approach (Calise et al., 2004, Calise et al., 2006 a-c). The following step of the research was the implementation of a finite-volume, axial-symmetric model of the SOFC stack, aimed at determining the profile of

* An initial version of this paper was published in July of 2006 in the proceedings of ECOS'06, Aghia Pelagia, Crete, Greece.
** Author to whom correspondence should be addressed.

the most important design and operating parameters within the SOFC component and to assess the error due to the above mentioned simplifying assumptions (Campanari et al., 2004, Stiller et al., 2005). However, even in these papers a few simplifying assumptions were used, with reference to polarizations (for example, concentration is neglected in Stiller et al., 2005 and Ohmic overvoltage is calculated on the basis of a simplified series electrical arrangement in Campanari et al., 2004) and reforming reactions. In this paper, a novel approach for the axial-symmetric simulation of the SOFC tube is presented, taking into account the most detailed models available for polarizations, chemical kinetics and pressure drops. In the following, the simulation model is briefly presented, paying special attention to the results provided by the simulation.

2. System configuration

SOFC can convert the chemical energy of natural gas directly into electricity by means of the combined mechanisms of steam methane reforming and electrochemical reactions. In particular, the steam reforming process is achieved by using the steam produced by the electrochemical reaction (Singhal et al., 2003). In fact, the mixture required to support the steam methane reforming reaction can be easily created by re-circulating SOFC anode outlet (Calise et al., 2006 c) 0.

In this paper, a SOFC stack with anode re-circulation arrangement is investigated. This system consists of a number of sub-components such as: SOFC tubes, catalytic burner, mixers, ejectors, pre-reformer and heat exchangers (Calise et al., 2006 c). The operating principle of the internal reforming SOFC stack, equipped with an anode recirculation arrangement, was widely described in a number of previous papers (e.g. Calise et al., 2006 c).

SOFC tube is displayed in *Figure 1*, whereas its pre-reformer is shown in *Figure 2*. This latter component consists of a shell with a number of tubes filled with a proper catalyst for the steam methane reforming reactions. The heat required to support such reaction is supplied by the hot gases coming from the outlet of the stack combustor. Obviously, the stream coming out from the pre-reformer tubes is directly brought to the SOFC anode inlet.

In this work, the analysis is carried out only for the pre-reformer and SOFC tube that can be considered as the most complex components. Boundary conditions (air and fuel inlet temperature and chemical compositions) are derived from works previously developed by the authors (Calise et al., 2006 c). In future works, the 1-D model will be extended to the entire SOFC stack.

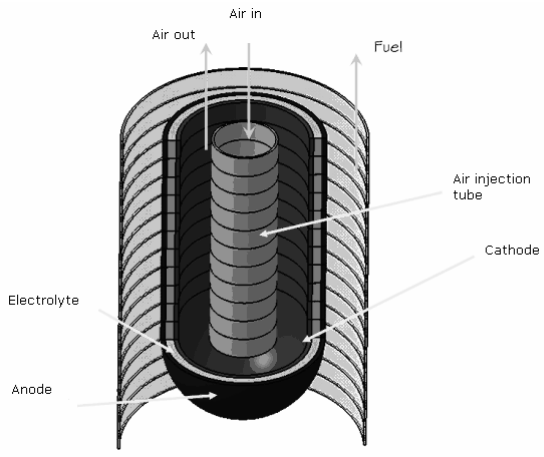

Figure 1. SOFC Tubular arrangement.

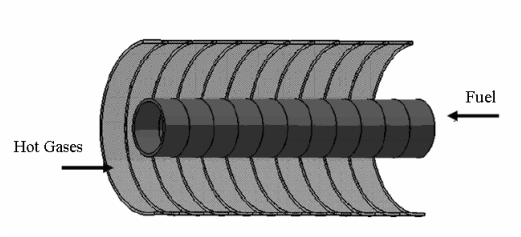

Figure 2. Pre-reformer configuration.

3. Electrochemical Model

SOFC voltage depends on a number of parameters, such as temperature, pressure, anode, cathode, electrolyte and interconnection thicknesses, porosity and tortuosity, materials, geometrical peculiarities, inlet chemical compositions, etc (Stiller et al., 2005). In order to consider all these factors, a detailed simulation model must be implemented. One of the aims of this paper is the development of a detailed simulation model to be used in order to verify the correctness of the simplifying assumptions, usually adopted in SOFC simulations. Previous works showed that some common simplifications, such as the use of the Tafel equation for the activation overvoltage or the use of the Fick's Law for the concentration polarization, should be avoided, since they may lead to significant errors, as shown in (Chan et al., 2001) and (Calise et al., 2004), respectively. In the present paper, detailed models for all the polarizations were implemented, as described in the following.

Obviously, cell voltage can be calculated evaluating Nernst open circuit reversible voltage (Larmine et al., 2004) and all the polarizations, according to the equation:

$$V = \frac{-\Delta\bar{g}_f^0}{2F} + \frac{RT}{2F}\ln\frac{p_{H_2}\,p_{O_2}^{1/2}}{p_{H_2O}} - \\ -\eta_{act,A} - \eta_{act,C} - \eta_{conc,A} - \eta_{conc,C} \quad (1)$$

Electron and ions transfer, respectively through electrodes and electrolyte, determine a loss due to their resistivities. Such property can be easily related to the operating temperature by means of exponential semi-empirical equations (Calise et al., 2006 a). Nevertheless, the calculation of the overall electric resistance is very complex since charges and ions flows occur both in radial and circumferential directions. Thus, the typical simplification of assuming a radial flow for electrons and ions (e.g.: Costamagna et al., 2001) was here avoided, by implementing more accurate relations such as those developed in (Nisancioglu, 1989). The activation overvoltage, due to the energy barrier to be overcome to activate the electrochemical reaction, is evaluated by means of the well-known Butler-Volmer (Calise et al., 2006 c). The exchange current densities (Singhal et al., 2003) are exponential function of temperature, are given in (Calise et al., 2006 c). Finally, the concentration overvoltage is due to the diffusion resistance of the porous media (anode and cathode). This phenomenon causes lower values of hydrogen and oxygen partial pressures, at the Three Phase Boundary, with respect to their corresponding values in the external flow (Larmine et al., 2004). Such overvoltage is related to the porosity of the electrodes and to the diffusion properties of the reacting mixtures (Chan et al., 2001). Usually, in the finite-volume simulation of SOFC the concentration overvoltage is neglected, since it is two orders of magnitude lower than other overvoltages, and modelling the concentration polarization is quite complex (Stiller et al., 2005). However, this assumption holds true only when the operating current density is lower than the corresponding limiting value 0. (Larmine et al., 2004) Hence, in some operating conditions (large values of the fuel utilization factor), the concentration overvoltage may become as large as the Ohmic and activation polarizations, as shown in Calise et all (2006 c). Thus, a complete polarization model should also include the concentration overvoltage in order to show all the phenomena that could occur in the SOFC tube (Chan et al., 2001). In this paper, the diffusion was considered as a combined mechanism of ordinary binary diffusion and Knudsen diffusion (Chan et al., 2001). The binary diffusion coefficient can be calculated on the basis of the Chapman-Enskog theory, also including the Lennard-Jones intercollision integral (Reid, 1977):

$$D_{AB} = 1{,}858 * 10^{-3} T^{3/2} \frac{\left[\frac{M_A + M_B}{M_A M_B}\right]^{1/2}}{p\sigma_{AB}^2 \Omega_D} \quad (2)$$

$$\Omega_D = \frac{A}{\left(\frac{kT}{\varepsilon_{AB}}\right)^B} + \frac{C}{\exp\left(D\frac{kT}{\varepsilon_{AB}}\right)} + \\ \frac{E}{\exp\left(F\frac{kT}{\varepsilon_{AB}}\right)} + \frac{G}{\exp\left(H\frac{kT}{\varepsilon_{AB}}\right)} \quad (3)$$

Knudsen diffusion coefficient can be calculated on the basis of the theory of diffusion in a cylindrical pore, by means of the average pore radius, that can be related to the porosity, porous media area and bulk density (Reid, 1977; CEIC0010; Todd et al., 2002):

$$D_K = 97{,}0\bar{r}\sqrt{\frac{T}{M}} = 97{,}0\frac{2\varepsilon}{S_A\rho_B}\sqrt{\frac{T}{M}} \quad (4)$$

The actual overall diffusion coefficient can be calculated by considering material porosity and tortuosity and the combined mechanisms of ordinary and Knudsen diffusion, according with equation (5).

$$\frac{1}{D_{A,eff}} = \frac{\xi}{\varepsilon}\left(\frac{1}{D_{AB}} + \frac{1}{D_{AK}}\right) \quad (5)$$

Finally, the above calculated diffusion coefficient can be used in concentration equations in order to evaluate anode and cathode concentration over-potentials. In this paper, the theory developed by Chan et al. was used in order to evaluate both anode and cathode concentration overvoltages (Chan et al., 2001).

4. Reforming and Internal Reforming Model

The simulation of the reforming and internal reforming processes is usually carried out by implementing semi-empirical equations for the kinetic of the Steam Methane Reforming (SMR) reaction and by assuming equilibrium-controlled the shift reaction (Calise et al., 2006 c). In order to avoid such simplifying assumption, in this paper a general theory, widely used in chemical process analysis, was implemented, by introducing relations that simultaneously include equilibrium and kinetic (Gallucci at al., 2004, Xu et al., 1989). This approach was used to simulate both pre-reforming and internal reforming processes. Furthermore, a special adjustment of the above

mentioned model was performed, in order to simulate the internal reforming process. In fact, such approach was developed for the simulation of industrial reformers equipped with tubes filled with a proper catalyst. Conversely, in the SOFC the reforming reaction occurs at the thin anode layer that also consists of Ni (catalysts for the reforming reaction). Thus, the above mentioned approach (Gallucci at al., 2004, Xu et al., 1989) was properly calibrated and modified for the SOFC configuration, using an equivalent catalyst bulk density, in order to consider the catalyst mass that really participates in the reforming process. According to this approach, the SOFC overall process (internal reforming and electrochemical reaction) consists of reactions (6) to (9), whereas the pre-reforming process is carried out by reactions (6) to (8):

$$CH_4 + H_2O \Leftrightarrow CO + 3H_2 \quad (6)$$

$$CO + H_2O \Leftrightarrow CO_2 + H_2 \quad (7)$$

$$CH_4 + 2H_2O \Leftrightarrow CO_2 + 4H_2 \quad (8)$$

$$H_2 + \frac{1}{2}O_2 \rightarrow H_2O \quad (9)$$

The rate of reaction (8) can be determined on the basis of the electrochemical model, as described in the following, whereas the rate of the three reforming reactions must be evaluated on the basis of the equations (10) to (14):

$$r_1 = \frac{\frac{k_1}{p_{H_2}^{2,5}}\left[p_{CH_4}p_{H_2O} - \frac{p_{H_2}^3 p_{CO}}{K_{eq_1}}\right]}{DEN^2} \quad (10)$$

$$r_2 = \frac{\frac{k_2}{p_{H_2}}\left[p_{CO}p_{H_2O} - \frac{p_{H_2}p_{CO_2}}{K_{eq_2}}\right]}{DEN^2} \quad (11)$$

$$r_3 = \frac{\frac{k_3}{p_{H_2}^{3,5}}\left[p_{CH_4}p_{H_2O}^2 - \frac{p_{H_2}^4 p_{CO_2}}{K_{eq_3}}\right]}{DEN^2} \quad (12)$$

$$DEN = 1 + K_{CO}p_{CO} + \\ + K_{H_2}p_{H_2} + K_{CH_4}p_{CH_4} + K_{H_2O}\frac{P_{H_2O}}{P_{H_2}} \quad (13)$$

$$k_i = A_i \exp\left(\frac{-E_i}{RT}\right) \quad (14)$$

The coefficients of equation (13) are given in literature (Gallucci at al., 2004, Xu et al., 1989). Equilibrium constants were calculated on the basis of the model previously developed by the authors (Calise et al., 2006 c). The rate of the electrochemical reaction was calculated on the basis of the electrochemical model, discussed in section 0. In fact, fixed the cell operating voltage, the polarization curve can be inverted in order to calculate current density. Such value can be used in a mole balance in order to evaluate the rate of the electrochemical reaction (Singhal et al., 2003):

$$r_4 = \frac{iA_{cell}}{2F} \quad (15)$$

Finally, from the above mentioned rates of reactions (equations from (9) to (14)), the outlet chemical composition were evaluated, by means of mole balances.

5. Pressure drops and heat exchange coefficients model

In this paper a pressure drop model was also included, based on the calculation of the friction factor depending on the Reynolds number. Correlations for friction factor are given in literature for all the streams included in the SOFC (Calise et al., 2006 c). The calculation of all the thermophysical properties (conductivity, viscosity, density, enthalpy, entropy, etc.) was based on the model previously developed by the authors (Calise et al., 2006 c). Similarly, correlations for the Nusselt number were implemented in order to evaluate all the heat exchange coefficients.

6. SOFC and pre-reformer discretizations and heat exchange models

In order to evaluate the profile of the most important parameters within the pre-reformer and the SOFC tube, such components were discretized along their axes, as shown in *Figure 3* and *Figure 4*.

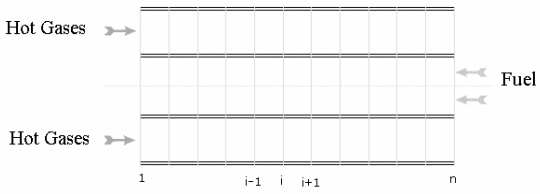

Figure 3. Pre-reformer discretization.

The typical tubular configuration of the SOFC, developed by Siemens is shown in *Figure 1*. The system consists of the cell, i.e. anode, cathode and electrolyte, and of an air injection tube required to supply air to the cathode compartment of the fuel cell. In this paper, a finite-volume axial-symmetric steady simulation of the SOFC tube was implemented. Consequently, border effects due to change of air flow direction in the bottom were neglected.

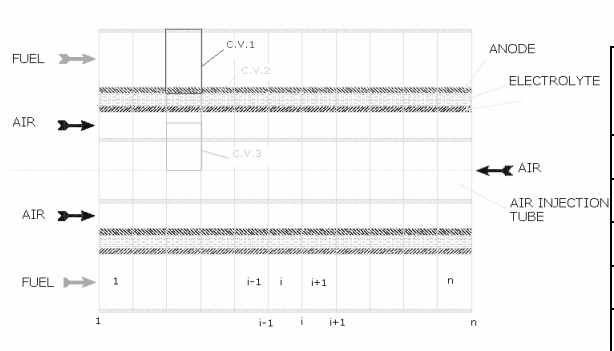

Figure 4. SOFC tube discretization.

The overall control volume was discretized by means of slices obtained with n plans orthogonal to the axis of the cylinders. Thus, the system was divided into $n - 1$ slice (see *Figure 4*). The slice can be considered as the elementary volume of the discretization, and is reported on the x-axis of the following figures.

Similarly, the discretization of the pre-reformer was carried out.

Appropriate algorithms, written in MATLAB and TOMLAB, were developed both for SOFC tube and pre-reformer in order to determine the profiles of all the thermodynamic, chemical and electrical properties within those components. These algorithms were based on the above discussed chemical, electrochemical and pressure drops models coupled with the energy balance equations.

7. Results and discussion

7.1 Pre-reformer

In theory, SOFC can also operate with a full internal reforming, i.e.: without any pre-reforming process. However, this circumstance should always be avoided, since the use of a pre-reformer provides several benefits. In fact this component is required to crack the higher hydrocarbons included in the fuel; in addition the pre-reforming promotes the internal reforming process and the electrochemical reaction. In fact, a cell not equipped with a pre-reformer would not produce any current at its bottom, since the corresponding active area would be used for the reforming process and not for the electrochemical reaction. It is also well-known that the reforming process occurring in the pre-reformer is strongly endothermic, resulting in a dramatic decrease of the fuel temperature. In fact the reforming process is much faster than the heat exchange between the reacting stream and the hot gases, determining the temperature profiles shown in *Figure 5*. Here, the active pre-reforming area is clearly detectable (from slice 80 to 100), also showing that the hot gases temperature variation is very low. In fact, the heat required to support the endothermic reforming process is mainly supplied by the convective flow of the reforming stream.

TABLE I. INLET MOLAR FLOW RATES.

	SOFC		PR	
	Air	**Fuel**	**Hot Gases**	**Fuel**
H_2O (%)	0.0	26.8	8.8	44.4
CO (%)	0.0	11.1	0.0	4.8
H_2 (%)	0.0	33.3	0.0	7.1
O_2 (%)	21.0	0.0	11.3	0.0
N_2 (%)	79.0	0.6	75.5	0.8
CO_2 (%)	0.0	18.3	4.4	20.6
CH_4 (%)	0.0	9.8	0.0	22.2
tot (kmol/s)	3.75E-05	1.51E-06	1.02E-03	2.52E-04

All the results described in the following were calculated on the basis of the parameters fixed in TABLE I and TABLE II.

TABLE I shows the molar flow rate and chemical composition of inlet streams. Such data were calculated using the 0-D model previously developed by some of the authors (Calise et al., 2006 c, Calise et al., 2004). TABLE II shows the geometrical and operating parameters, which are similar to those of Siemens SOFC systems (Calise et al., 2004).

It is also well-known that high temperature gradients in the SOFC must be avoided. Thus, it is not possible to feed the stack with low temperature air and fuel. The air inlet temperature can be increased by means of an external pre-heater, supplied by the SOFC outlet stream. On the other hand, the fuel can be pre-heated by increasing the length of the pre-reformer, since this component also acts as a tube-in-tube counter-flow heat exchanger. However, the larger the length of the pre-reformer, the higher is the demethanization rate achieved in the same component.

Therefore, an increase in the pre-reformer length would result in a better heat exchange but also in a complete reforming process within such component. This circumstance must be avoided, since the internal reforming is crucial to provide additional cooling to the stack, avoiding unacceptable values of the stack temperature. Therefore, in the system under analysis the heat exchange was improved by adding a counter-flow heat exchange between the hot gases and the fuel, in series with the pre-reforming process, as shown in *Figure 5*. Here, it is also shown that a simple heat exchange process occurs in slices from 1 to 80, whereas combined heat exchange and steam reforming processes take place at slices from 81 to 100. This arrangement was achieved by filling with catalyst only a part of the pre-reformer tubes (slices from 81 to 100), so reducing their active length.

TABLE II. FIXED PARAMETERS.

Parameter	Unit	Value
Pre-reformer length	m	1.5
Pre-reformer active length	m	0.30
Pre-reformer fuel inlet temp.	°C	900
Pre-reformer hot gases inlet temp.	°C	1070
Pre-reformer tube diameter	cm	1.56
Pre-reformer wall thickness	cm	0.10
Pre-reformer catalyst bulk density	kg/m3	1200
Cell Voltage	V	0.620
Anode thickness	cm	0.010
Cathode thickness	cm	0.220
Electrolyte thickness	cm	0.004
Interconnection thickness	cm	0.0085
Cell length	m	1.50
Interconnection versus cell area	/	0,097
Fuel inlet pressure	bar	3.00
Air inlet pressure	bar	3.00
SOFC Equivalent ρ_b	kg/m3	0.60
Air inlet temperature	°C	900
Cell diameter	cm	1.56
Injection tube diameter	cm	1.20
Anode pore diameter	m	$0.5\ 10^{-6}$
Cathode pore diameter	m	$0.5\ 10^{-6}$
Anode porosity	%	50
Anode tortuosity	/	5.90
Cathode porosity	%	50
Cathode tortuosity	/	5.90
Anode conductivity	W/m K	2.00
Cathode conductivity	W/m K	2.00
Electrolyte conductivity	W/m K	2.00
Interconn.conductivity	W/m K	2.00

A simple energy balance returns that the higher the demethanization rate, the higher is the amount of heat required by the pre-reforming process. Reforming reaction kinetics are shown in *Figure 7*, where it is clearly displayed that the rate of the shift reaction, not equilibrium controlled as usually assumed, is mainly negative, whereas the reforming Steam Methane Reaction (eq. (5)) is much faster than the demethanization (eq. (8)). *Figure 7* also shows that the steam methane reforming reactions are far from the chemical equilibrium. In fact, the chemical composition of the stream exiting the pre-reformer is very different from that of equilibrium. In addition, *Figure 7* clearly shows that, at the pre-reformer outlet, steam methane reforming reactions are still in progress. Pressure profile plots are omitted since pressure drops are negligible. It is important to emphasize that the results achieved in *Figure 7* could not be achieved by 0-D models.

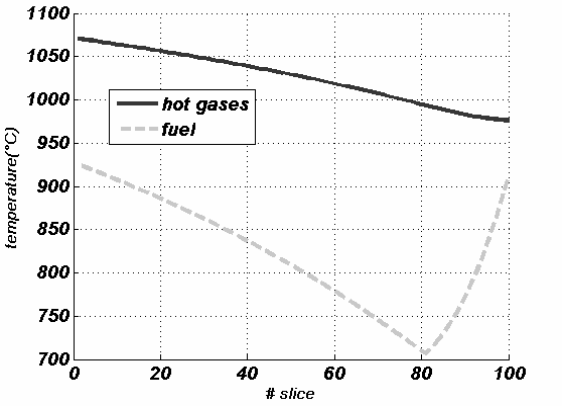

Figure 5. Pre-reformer temperatures.

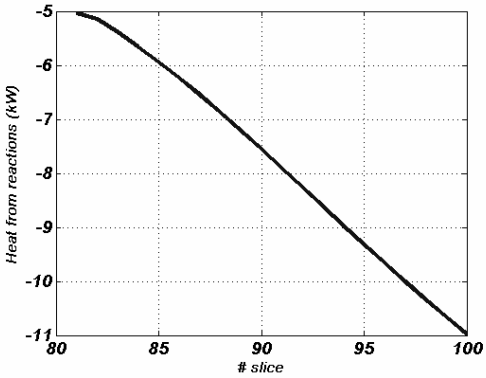

Figure 6. Pre-reformer heat from reactions.

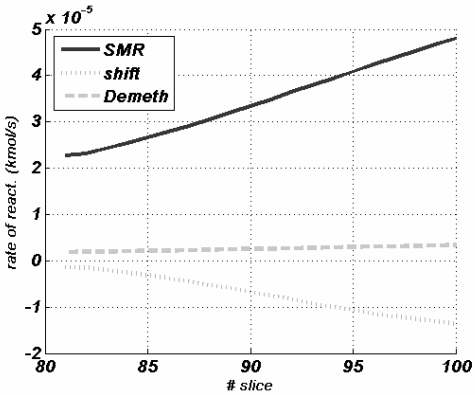

Figure 7. Pre-reformer reaction rates.

7.2 SOFC tube

Figure 8 shows that, in the first part of the SOFC tube, the reforming process is faster than the electrochemical one. Then, the reforming reactions reach very quickly to the equilibrium conditions (rates of reaction asymptotically approaching zero), whereas the electrochemical reaction continues to occur, depending on the shape of the polarization curve. Obviously, higher the cell operating voltage, lower the corresponding current density, i.e.: slower the electrochemical process. Conversely, the rates of

the reforming reactions are basically related to the temperature and partial pressure fields.

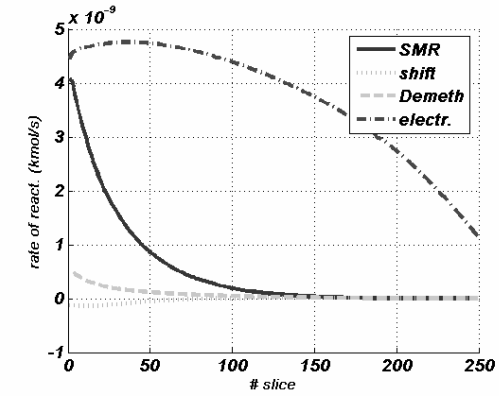

Figure 8. SOFC reaction rates.

The profile achieved in *Figure 8* is much more detailed than those typically returned by 0-D models. In fact, in this case the calculation of chemical/electrochemical reaction rates is related to the local thermodynamic properties, whereas, in 0-D models, average values of the thermodynamic properties must be used (Calise et al., 2006 c). The rates of the four reactions (Gallucci et al., 2004) affect the trend of the heat produced by the overall chemical-electrochemical process (*Figure 9*). In fact, at first, the reforming reaction is faster than the electrochemical one. Consequently, the heat generated by the hydrogen electrochemical oxidation is lower than that required by the reforming reactions. Then, the heat generated by the electrochemical reaction is much larger than that required by the internal reforming. Finally, in the last sections of the tube, the overall generated heat decreases, as a consequence of the reduction of the electrochemical rate of reaction. Furthermore, the shape of the current density function, displayed in *Figure 10*, is strictly related to the hydrogen availability, since the open circuit reversible voltage, and the activation and concentration overvoltages mainly depend on the hydrogen partial pressure. The SOFC under investigation is dramatically affected by the ohmic polarization.

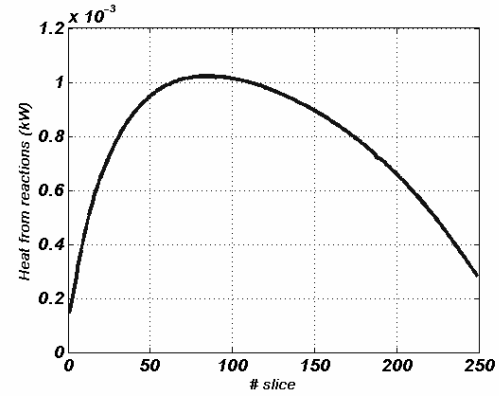

Figure 9. SOFC heat from reactions.

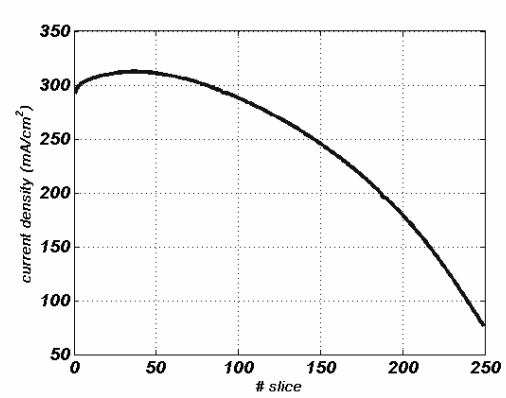

Figure 10. Current density.

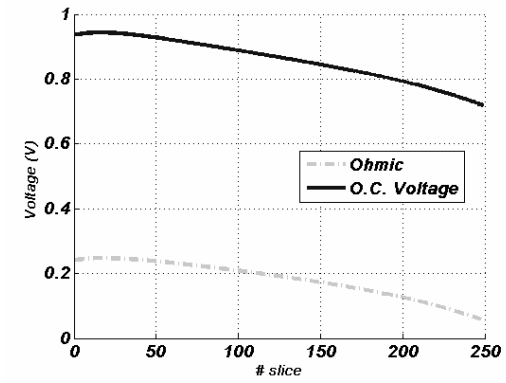

Figure 11. Nernst potential and Ohmic Overvoltage.

Figure 11 clearly shows that the Ohmic overvoltage is much higher than all other losses. The trend of the ohmic polarization curve reproduces the shape of the solid temperature (*Figure 13*). In fact, the higher the slice temperature, the lower the corresponding ohmic polarization. On the other hand, *Figure 11* also shows the shape of the Nernst open circuit reversible voltage, dramatically depending on hydrogen, oxygen and water partial pressures. Thus, Nernst potential decreases since: H_2 and O_2 partial pressures decrease since those components are consumed by the electrochemical reaction whereas H_2O partial pressure increases since it is produced by the electrochemical reaction. *Figure 12* shows the activation and concentration overvoltages in the SOFC tube. At first, the magnitude of the concentration overvoltage is much lower than the other polarizations. In addition, the cathodic concentration overvoltage is predominant on the anodic one. The trend of concentration overvoltage at the cathode is due to the shape of the current density displayed in *Figure 10*. Finally, the shape of the activation overvoltage is basically due to the solid temperature, displayed in *Figure 13*. In fact, the higher the operating temperature, the lower the corresponding activation overvoltage. In this case, this phenomenon is dominant over the reduction of hydrogen and oxygen partial pressures.

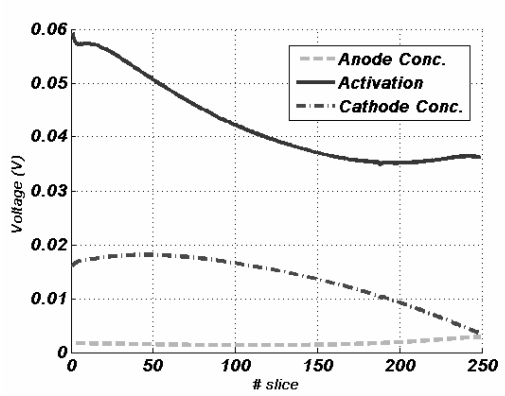

Figure 12. Concentration and activation overvoltages.

The result of the calculation of temperature fields is shown in *Figure 13*, as above discussed. The air enters the injection tube (slice 250, air injection stream), where it is preheated up to 942 °C (slice 1). Then, the air passes through the cathode compartment, with a change in the flow direction (slice 1, air cathode stream), exiting the cell at 968 °C (slice 250). On the other side, the temperatures of fuel inlet (slice 1, fuel stream) and outlet (slice 250, fuel stream) are 921 °C and 973 °C, respectively. So, the typical simplification of assuming the same temperature value for air and fuel outlet streams is not completely justified. In addition, *Figure 13* shows that the SOFC cannot be considered isothermal, as usually assumed by a number of authors in simplified 0-D models.

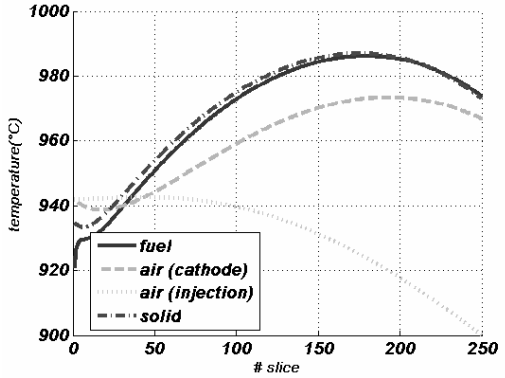

Figure 13. SOFC temperatures.

Moreover, the optimum temperature profiles, displayed in *Figure 13*, were achieved by handling the following parameters: pre-reformer demethanization rate, air to fuel ratio, air and fuel inlet temperatures, cell and injection tube diameters. Temperature curves are also influenced by the air to fuel ratio. In fact, the air mass flow rate is much higher than the stoichiometric value, in order to provide the appropriate stack cooling. Such cooling could also be achieved by lowering the air inlet temperature. However, in this case, remarkable temperature gradients along the SOFC tube axis would be achieved. All pressure drops in are low, and can be neglected. In particular, a slight pressure drop is perceptible only for the cathodic stream, as a consequence of the high mass flow rate and velocity.

Finally, *Figure 14* shows the fuel molar flow rates along the SOFC axis, also putting in evidence the trend of the chemical and electrochemical phenomena occurring in the SOFC tube. In fact, in the first part of the SOFC the internal steam reforming process is dominant over the electrochemical reaction, inducing an increase of the hydrogen partial pressure. Conversely, in the same section the steam partial pressure decreases, because the amount of water used by the internal reforming process is much higher than the one released by the electrochemical process. Then, the steam reforming reactions quickly approach the equilibrium conditions, as clearly shown in *Figure 14*, since CO, CO_2, CH_4 curves are flattening. In particular, the methane molar flow rate approaches the value of 0 kmol/s from the 20th slice of the control volume. This result shows that the high operating temperatures of the SOFC and its chemical and geometrical peculiarities permit to consume all the inlet methane within the cell. Conversely, the partial pressures of H_2 and H_2O decrease and increase, respectively, as a consequence of the progress of the electrochemical reaction.

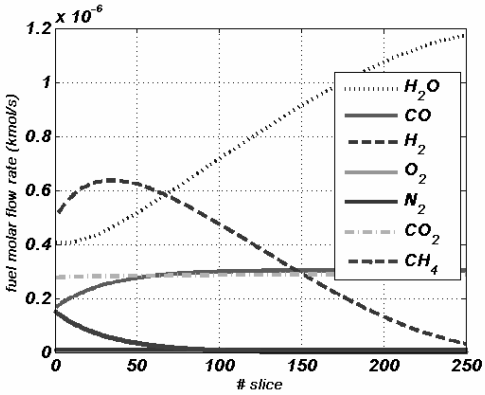

Figure 14. SOFC fuel molar flow rates.

The cell under investigation also shows a good chemical design. In fact, the overall fuel utilization factor approaches the value of 81 % accordingly with manufacturer requirements (Singhal et al., 2003). In fact, higher fuel utilization factor would need much higher cell active area, dramatically increasing SOFC capital costs. Obviously, the unreacted fuels can be usefully used in a combustor to provide the heat required to preheat inlet air and fuel steams

8. Conclusion

This paper presents an original approach for the finite-volume axial-symmetric simulation of a tubular SOFC. The simulation model presented allows accurate calculation of the main physical,

chemical, electrical and electrochemical properties in the system, such as temperature, pressure, chemical composition, overvoltages, current, etc. Such approach includes a number of detailed models for the calculation of electrochemistry and of the kinetics of the internal reforming process, that were properly calibrated in order to comply with the SOFC experimental data (Calise et al., 2006 c). The results showed that some of the simplifying assumptions usually adopted in SOFC simulations are not rigorously acceptable, e.g.: the generator is not isothermal, concentration overvoltages cannot be considered negligible for whatever operating condition, the shift reaction is not equilibrium-controlled, etc. The computer code presented in the paper will be the basis for more detailed analysis of the SOFC tube and of the stack in general, such as simulation of a complete stack and of hybrid plants and thermo-economic optimizations of the stack.

Nomenclature

V	Cell Voltage (V)
g_f	Gibbs free energy (kJ/kmol)
F	Faraday constant
R	Gas constant (kJ/kmol K)
p	Partial pressure (bar)
h	Overvoltage (V)
d	Thickness (m)
L	Length (m)
i	Current density (mA/cm^2)
D_{AB}	Binary diffusion coefficient
M	Molar mass (g/mol)
e	Porosity
x	Tortuosity
Ω_D	Lennard-Jones intercollision integral
σ_{AB}	Lennard-Jones characteristic length (Å)
ρ_B	Bulk density (kg/m^3)
S_A	Pore area (m^2)

References

Calise F., Dentice d'Accadia M., Palombo A., Vanoli L., 2006, *Simulation and exergy analysis of a SOFC-gas turbine system, Energy: the international Journal* , Volume: 31, Issue: 15, December, 2006, pp. 3278-3299

Calise F., Palombo A., Vanoli L., 2006, *Design and partial load exergy analysis of a hybrid sofc-gt power plant*, Journal of power sources, Volume: 158, Issue: 1, July 14, 2006, pp. 225-244

Calise F., Dentice d'Accadia M., Vanoli L., von Spakovsky M.R., 2006, *Single-Level Strategy for the optimal Sintheses/design of a Hybrid SOFC-GT Power Plant*, Journal of Power Sources, Volume: 159, Issue: 2, September 22, 2006, pp. 1169-1185

Calise F., Dentice d'Accadia M., Palombo A., Vanoli, L., Vanoli, R., 2004, *Modelling, simulation and exergy analysis of a hybrid SOFC -Gas Turbine System*. 3rd International Symposium Energy and environment 2004, Sorrento, 30th September to 2nd October.

Campanari S., Iora P., 2004, *Definition and sensitivity analysis of a finite volume SOFC model for a tubular cell geometry*, Journal of Power Sources 132 (2004) 113—226

Chan, S. H., Low, C. F. , Ding, O. L., 2002, *Energy and exergy analysis of a simple solid – oxide fuel cell power system.*, Journal of Power Sources, vol. 103, pp.188-200.

Chan, S.H., Ho, H.K.,Tian, Y., 2003, *Multi-level modelling of SOFC-gas turbine Hybrid system*, International Journal of Hydrogen Energy 28 (2003) 889-900.

Chan S.H., Kior K.A., Xia, Z.T., 2001, *a complete polarization model of a solid oxide fuel cell and its sensitivity to the change of cell component thickness*, Journal of Power Sources 93 (2001) 130-140

Costamagna, P., Magistri, L., Massardo, A., 2001, *Design and part-load performance of a hybrid system based on a solid oxid fuel cell reactor and a micro gas turbine*, Journal of Power Sources 96 (2001) 352-368.

CEIC0010, *Diffusion vs Mass Transfer by Bulk Motion, Fick's Law and Mass transfer rate equation*.

Fuel cell handbook (sixth edition), 2002, U.S. Departement of Energy.

Gallucci, F., Paturzo, L. , Basile, A. , 2004, *A simulation study of the steam reforming of methane in a dense tubular membrane reactor*, International Journal of Hydrogen Energy, vol. 29, pp. 611 – 617.

Larminie, J., Dicks, A., 2004, *Fuel cell system explained*, John Wiley & sons LTD.

Nisancioglu*, K., 1989, Natural gas fuelled solid oxide fuel cells and systems, ohmic losses*, Workshop on mathematical modelling, Charmey/Switzerland, july 2 to 6 1989.

Reid, Prausnitz, *The Properties of gases and liquids,* Mc Graw Hill, 1977

Stiller, C., Thorud, B., Seljebo, S., Mathisen, O., Karoliussen, H., Bolland, O., 2005, *Finite volume modelling and hybrid-cycle performance of planar and tubular solid oxide fuel cells*, Journal of Power Sources 141 (2005) 227-240.

Singhal, S.C., Kendall, K., 2003, *High temperature Solid Oxide Fuel Cells*, Elsevier.

Todd B., Young J.B., 2002, *Thermodynamic and transport properties of gases for use in solid oxide fuel cell*, Journal of power Sources 110 (2002) 186-200

Xu, J., Froment, G. F., 1989, *Methanes-steam reforming: methanation and water-gas shift: I. Intrinsic kinetics*, AlXhE Journal, vol.35 no.1.

Chemical Properties Handbook, 1999, McGraw Hill, pp. 531-556.